Quantum-state-preserving optical frequency conversion and pulse reshaping by four-wave mixing

C. J. McKinstrie,[1,*] L. Mejling,[2] M. G. Raymer,[3] and K. Rottwitt[2]

[1]*Bell Laboratories, Alcatel-Lucent, Holmdel, New Jersey 07733, USA*
[2]*Department of Photonics, Technical University of Denmark, 2800 Kongens Lyngby, Denmark*
[3]*Department of Physics, University of Oregon, Eugene, Oregon 97403, USA*

Nondegenerate four-wave mixing driven by two pulsed pumps transfers the quantum state of an input signal pulse to an output idler pulse, which is a frequency-converted and reshaped version of the signal. By varying the pump shapes appropriately, one can connect signal and idler pulses with arbitrary durations and shapes. This process enables a variety of functions required by quantum information networks.

In conventional communication networks, classical information is transported by optical pulses. In a coherent channel, information is encoded in the pulse amplitudes and phases. One can increase the rate at which information is transported by multiplexing channels in frequency, polarization, pulse shape or time [1,2]. To operate multichannel networks efficiently, one should be able to insert (add) information to, and extract (drop) information from, specific channels and transfer (reroute) information between different channels.

A key requirement of quantum information networks is the ability to transport quantum states between nodes [3,4]. These nodes (material-based quantum memories with resonance wavelengths in the range 300–800 nm) could be nearby (in the same device) or distant (linked by optical fibers with low-loss windows centered on 1310 or 1550 nm). Their resonance wavelengths could be the same, or similar, or could differ significantly. Furthermore, the durations and shapes of pulses emitted by quantum memories differ significantly from the short bell-shaped pulses favored by communication systems. To optimize the transmission of quantum information, the ability to frequency convert (FC) and reshape optical pulses, while preserving their quantum states, is essential. This ability also enables new physical paradigms, such as the modification of two-photon Hong-Ou-Mandel (HOM) interference [5–7] and photon concealment [8].

Quantum-state-preserving FC is enabled by three-wave mixing (TWM) in a crystal [9,10]. In this process, a strong pump wave (p) couples weak signal (s) and idler (r) waves. (At the photon level, $\pi_s \longleftrightarrow \pi_p + \pi_r$, where π_j represents a photon with carrier frequency ω_j.) Recently, it was shown theoretically that TWM, in conjunction with spectral phase modulation and propagation [11], or dispersion engineering [12], can connect pulses with disparate durations (quasicontinuous waves are converted to short pulses, or *vice versa*). However, TWM is limited in practice to large frequency shifts, which prevents its use for FC within the telecommunication bands.

Quantum-state-preserving FC is also enabled by four-wave mixing (FWM) in a fiber [13,14]. In the nondegenerate FWM process called Bragg scattering (BS), which is illustrated in Fig. 1, two pump waves (p and q) couple signal and idler waves, whose frequencies differ by arbitrary amounts

($\pi_s + \pi_p \longleftrightarrow \pi_q + \pi_r$). BS has been used in conventional communication experiments to provide tunable intraband FC and multiplexing [15,16]. In this article, we show that BS also has the ability to reshape pulses (including single-photon wave packets) arbitrarily, without additional processing or dispersion engineering. This extra functionality is enabled by the presence of two pumps, which can be shaped independently. If single-photon states are used as qubits, information can be encoded in all but one of the aforementioned degrees of freedom (the coherent amplitude). If the input photon is entangled with another system, this entanglement is preserved by FC and reshaping. Examples include two-photon energy-time entanglement, the preservation of which was demonstrated in Ref. [3], and polarization entanglement, which is preserved by signal-polarization-independent BS [13].

BS is governed by the coupled-mode equations (CMEs)

$$(\partial_z + \beta_r \partial_t) a_r(z,t) = i\gamma_{pq}(z,t) a_s(z,t), \tag{1}$$

$$(\partial_z + \beta_s \partial_t) a_s(z,t) = i\gamma_{pq}^*(z,t) a_r(z,t), \tag{2}$$

where a_r and a_s are the annihilation operators of the idler and signal, respectively, β_r and β_s are the group slownesses (inverse speeds), and $\gamma_{pq}(t,z) = \gamma A_p(t - \beta_s z)A_q^*(t - \beta_r z)$ is the pump-induced coupling function [13]. These CMEs are based on the assumption that the carrier frequencies and wave numbers are matched. Pump p copropagates with the signal, whereas pump q copropagates with the idler [14]. If the waves are copolarized and each pump amplitude satisfies the normalization condition $\int |A_j(t)|^2 dt = 1$, the coupling coefficient $\gamma = 2\gamma_K (E_p E_q)^{1/2}$, where γ_K is the Kerr coefficient and E_j is a pump energy. The CMEs for cross-polarized waves are similar [13].
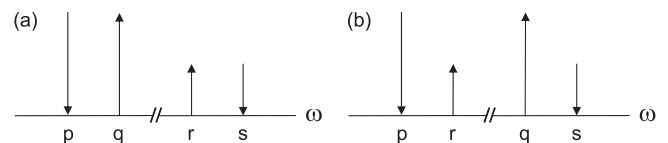

FIG. 1. Frequency diagram for (a) nearby and (b) distant Bragg scattering. Long arrows denote pumps (p and q), and short arrows denote idler and signal sidebands (r and s). Downward arrows denote modes that lose photons, whereas upward arrows denote modes that gain photons. The directions of the arrows are reversible.

*mckinstrie@alcatel-lucent.com

The solutions of the CMEs can be written in the input-output form,

$$a_j(l,t) = \sum_k \int_{-\infty}^{\infty} G_{jk}(l,t|0,t') a_k(0,t') dt', \qquad (3)$$

where G_{jk} is the Green (transfer) function that describes the effect on mode j at the output point (l,t) of an impulse applied to mode k at the input point $(0,t')$. These functions describe the properties of FC completely. Each Green function has the Schmidt decomposition [17]

$$G(t,t') = \sum_n v_n(t) \sigma_n^{1/2} u_n^*(t'), \qquad (4)$$

where $G(t,t')$ is an abbreviation for $G(l,t|0,t')$, u_n and v_n are input and output Schmidt modes (temporal eigenfunctions), respectively, and σ_n is a Schmidt coefficient (dilation factor). Furthermore, because FC is a unitary process, the Green functions and their decompositions are related by the matrix equation

$$\begin{bmatrix} G_{rr} & G_{rs} \\ G_{sr} & G_{ss} \end{bmatrix} = \sum_n \begin{bmatrix} v_{rn}\tau_n u_{rn}^* & v_{rn}\rho_n u_{sn}^* \\ -v_{sn}\rho_n^* u_{rn}^* & v_{sn}\tau_n^* u_{sn}^* \end{bmatrix}, \qquad (5)$$

where $|\tau_n|^2 + |\rho_n|^2 = 1$ [7]. If the sideband operators are decomposed in terms of Schmidt modes [$a_j(0,t') = \sum_n a_{jn}(0)u_{jn}(t')$], each pair of mode operators undergoes the beam-splitter-like transformation [18]

$$a_{rn}(l) = \tau_n a_{rn}(0) + \rho_n a_{sn}(0), \qquad (6)$$

$$a_{sn}(l) = -\rho_n^* a_{rn}(0) + \tau_n^* a_{sn}(0). \qquad (7)$$

If the input photon is prepared in the mode u_{sn}, the output photon will be in the mode v_{sn}, with probability $|\tau_n|^2$, or v_{rn}, with probability $|\rho_n|^2$.

For example, if the mode-conversion efficiency $|\rho_n|^2 = 1/2$, FC generates two-frequency entanglement: $|0_r\rangle|1_s\rangle \longrightarrow (|1_r\rangle|0_s\rangle + e^{i\phi}|0_r\rangle|1_s\rangle)/2^{1/2}$, where $|1_j\rangle$ represents a one-photon wave-packet state with carrier frequency ω_j, ϕ is a phase factor, and the mode number was omitted. It also enables two-frequency HOM interference [7]: $|1_r\rangle|1_s\rangle \longrightarrow (|2_r\rangle|0_s\rangle + e^{i\phi}|0_r\rangle|2_s\rangle)/2^{1/2}$. Alternatively, if $|\rho_n|^2 = 1$, FC enables quantum state translation: $|0_r\rangle|1_s\rangle \longrightarrow |1_r\rangle|0_s\rangle$. It also enables entanglement swapping: $(|1_s\rangle|\psi_a\rangle + e^{i\theta}|0_s\rangle|\psi_b\rangle)/2^{1/2} \longrightarrow (|1_r\rangle|\psi_a\rangle + e^{i\phi}|0_r\rangle|\psi_b\rangle)/2^{1/2}$, where $|\psi_a\rangle$ and $|\psi_b\rangle$ are two states associated with another subsystem. The Schmidt modes are the optimal input wave packets for these processes. Determining them allows one to optimize experiments or calculate the degradations associated with nonoptimal wave packets.

The CMEs are partial differential equations with space- and time-varying coefficients. Nonetheless, by using standard mathematical methods [19,20], one can solve them analytically for arbitrary pump shapes and strengths. The final results are

$$G_{rs}(t,t') = i\bar{\gamma} A_q^*(t - \beta_r l) J_0\{2\bar{\gamma}[\xi(t,t')\eta(t,t')]^{1/2}\} A_p(t')$$
$$\times H(t' + \beta_r l - t) H(t - t' - \beta_s l), \qquad (8)$$

$$G_{sr}(t,t') = i\bar{\gamma} A_p^*(t - \beta_s l) J_0\{2\bar{\gamma}[\xi(t,t')\eta(t,t')]^{1/2}\} A_q(t')$$
$$\times H(t' + \beta_r l - t) H(t - t' - \beta_s l), \qquad (9)$$

where $\bar{\gamma} = \gamma/(\beta_r - \beta_s)$ is the interaction strength, J_0 is a Bessel function of zeroth order, H is a Heaviside step function,

and the interaction distances

$$\xi(t,t') = \int_{t-\beta_r l}^{t'} |A_q(s)|^2 ds, \qquad (10)$$

$$\eta(t,t') = \int_{t'}^{t-\beta_s l} |A_p(s)|^2 ds. \qquad (11)$$

Only the cross functions G_{rs} and G_{sr} are considered in this article. However, since the cross functions are known, the self functions G_{rr} and G_{ss} can be determined by differentiation [Eqs. (1) and (2)], and once the Schmidt decompositions of the cross functions are known, the decompositions of the self-functions can be deduced [Eq. (5)].

In the low-strength regime ($\bar{\gamma} \ll 1$), $J_0 \approx 1$, and the cross functions [Eqs. (8) and (9)] are just products of the strength parameter, and the shape and step functions. If the sideband transit times ($\beta_j l$) are longer than the pump durations (τ_j), the step functions are 1 for times of interest: The cross functions are separable [$G_{rs}(t,t') = g_r(t)g_s(t')$], and the input and output Schmidt modes are just the conjugates of the shape functions. One can verify these results by using perturbation theory to solve the CMEs approximately. In the high-strength regime ($\bar{\gamma} > 1$) $J_0 \neq 1$, and the Schmidt modes differ from the shape functions.

The cross function G_{rs} is illustrated in Fig. 2 for cases in which $\bar{\gamma} = 0.1$, and the pumps have Gaussian shape functions
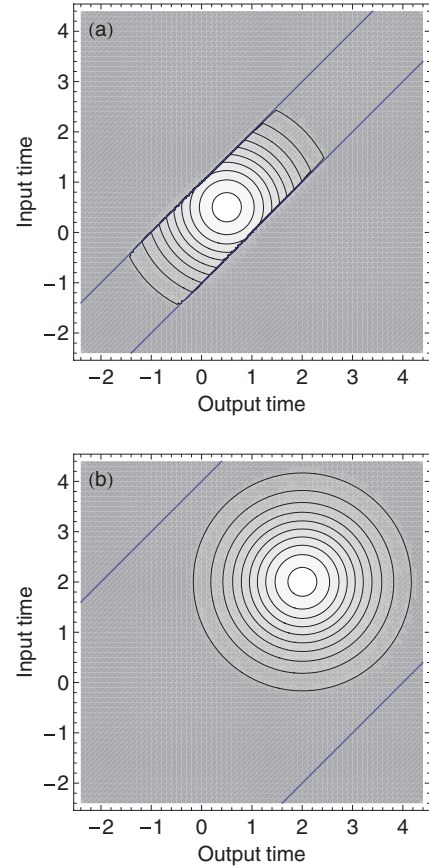

FIG. 2. (Color online) Contour plots of the Green function G_{rs} for the strength parameter $\bar{\gamma} = 0.1$ and the length parameters (a) $\beta l/\tau = 1$ and (b) $\beta l/\tau = 4$. The Green function is 0 outside the diagonal lines. Time is measured in units of τ.

with width τ and are timed to collide at the midpoint of the fiber. In a frame moving with the average slowness $\beta_a = (\beta_r + \beta_s)/2$, the relative slowness $\beta = \beta_r - \beta_a = -(\beta_s - \beta_a)$. Time and distance are measured in units of τ and τ/β, respectively. For fibers with intermediate lengths ($\beta l/\tau = 1$), the cross function is maximal at the collision point $(0.5, 0.5)$ and extends diagonally in the input-output plane. The abrupt cutoffs are caused by the step functions in Eq. (8), which impose causality and delineate the fiber boundaries. The absolute probability that an idler photon will be created always depends on the arrival time of the signal photon and the time interval during which the pumps collide. In this case, the relative probability that the idler photon will depart at a particular time depends strongly on the arrival time of the signal photon: The input and output times are correlated. For long fibers ($\beta l/\tau = 4$), the cross function is maximal at the collision point $(2, 2)$ and has circular contours. There is no abrupt cutoff because the pump-sideband collision takes place entirely within the fiber (is complete). In this case, the cross function is separable, and the input and output times are uncorrelated.

The square-root Schmidt coefficients ($|\rho_n|$) associated with G_{rs} are displayed in Fig. 3(a). For $\beta l/\tau = 1$, several coefficients have significant magnitudes, which is evidence of nonseparability. In contrast, for $\beta l/\tau = 4$, the lowest-order (first) coefficient is approximately 0.1, and the other coefficients are approximately 0.0, which is evidence of separability. The lowest-order Schmidt mode of the output idler is displayed in Fig. 3(b). For $\beta l/\tau = 4$, the idler mode equals $A_q^*(t - \beta_r l)$, as predicted by perturbation theory: It is an image of the input pump, conjugated and delayed by the transit time. [The input signal mode is $A_p^*(t')$.] For $\beta l/\tau = 1$,
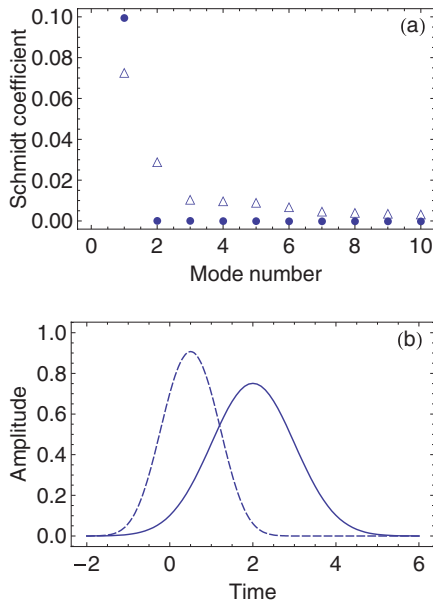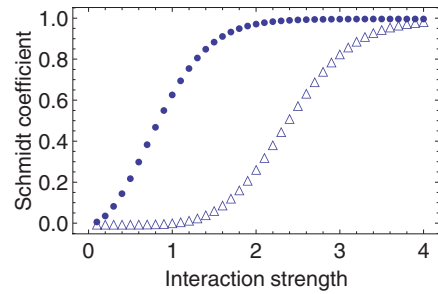

FIG. 4. (Color online) Schmidt coefficients ($|\rho_n|^2$) plotted as functions of the strength parameter ($\bar{\gamma}$). The solid circles denote $|\rho_1|^2$, and the hollow triangles denote $|\rho_2|^2$.

the Schmidt mode is taller and narrower than the pump, but is still bell shaped.

In the low-strength (low-conversion-efficiency) regime, the cross functions are separable if the fiber is sufficiently long, and one can FC and reshape signal pulses arbitrarily by varying the pump shapes. To determine whether these properties remain as the conversion efficiency increases, the cross function G_{rs} was decomposed numerically for the case in which $\beta l/\tau = 4$ (complete collision).

In Fig. 4, the first and second Schmidt coefficients ($|\rho_1|^2$ and $|\rho_2|^2$) are plotted as functions of the interaction strength ($\bar{\gamma}$). In the low-strength regime, the first coefficient (conversion efficiency) $|\rho_1|^2 \approx \bar{\gamma}^2$. In the high-strength regime, $|\rho_1|^2$ tends monotonically to 1 as $\bar{\gamma}$ increases, so complete conversion is possible. For efficiencies as high as 0.70, the value of the second Schmidt coefficient is no larger than 0.01, so the cross function is nearly separable: The first (target) Schmidt mode is converted with reasonable efficiency, whereas the other modes are unaffected. For higher efficiencies, the second coefficient increases rapidly, and the potential exists for intermodal crosstalk.

The lowest-order Schmidt mode of G_{rs} is displayed in Fig. 5 for the case in which $\beta l/\tau = 4$ and $\bar{\gamma} = 0.834$. These parameters correspond to a conversion efficiency of 50%, which is suitable for entanglement generation (which is optimized by phase-locked pumps) or HOM interference. The pumps are identical Gaussians, and the (common) Schmidt mode differs only slightly from the Gaussian predicted by perturbation theory. Numerical simulations, which include the effects of nonlinear phase modulation, show that the Schmidt
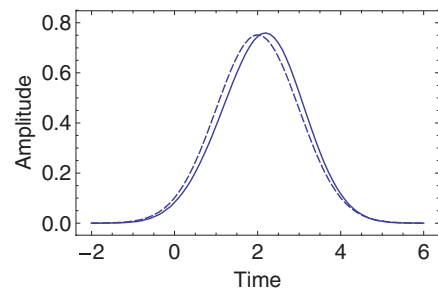

FIG. 3. (Color online) (a) Square-root Schmidt coefficients ($|\rho_n|$) of the Green function G_{rs} for the strength parameter $\bar{\gamma} = 0.1$ and the length parameters $\beta l/\tau = 1$ (hollow triangles) and $\beta l/\tau = 4$ (solid circles). (b) Lowest-order Schmidt mode plotted as a function of time (t/τ) for $\beta l/\tau = 1$ (dashed curve) and $\beta l/\tau = 4$ (solid curve).

FIG. 5. (Color online) Lowest-order Schmidt mode (solid curve) and (common) pump shape function (dashed curve) plotted as functions of time (t/τ) for the strength parameter $\bar{\gamma} = 0.834$.
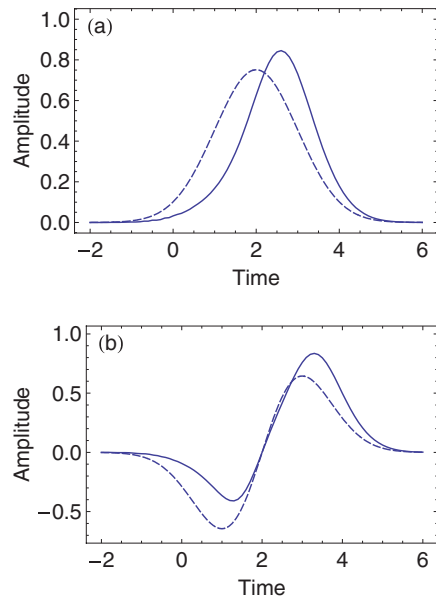
FIG. 6. (Color online) Lowest-order (a) signal and (b) idler Schmidt modes (solid curves) and pump shape functions (dashed curves) plotted as functions of time (t/τ) for the strength parameter $\bar{\gamma} = 1.544$.

modes are chirped, but are otherwise similar to the idealized modes described here [21].

The lowest-order Schmidt modes of G_{rs} are displayed in Fig. 6 for the case in which $\beta l/\tau = 4$ and $\bar{\gamma} = 1.544$. These parameters correspond to a conversion efficiency of 90%, which is high enough for reliable quantum FC or entanglement swapping. Pumps p and q are zeroth- and first-order Hermite-Gauss functions, respectively, so the wave packet is reshaped. The Schmidt modes are distorted Hermite-Gauss functions, as predicted by Eq. (8).

Speciality fibers exist with customizable dispersion, nonlinearity coefficients of 10–100/km-W, and lengths of 1–300 m. If $\beta = 0.7$ ps/m [14] and $\tau = 10$ ps, the required fiber length is 56 m, and the required pump powers are of order 1 W, so the proposed experiments are feasible.

In summary, BS driven by pulsed pumps was studied in detail. The Green functions and Schmidt decompositions associated with this FC process were determined for arbitrary signal-idler conversion efficiencies. Provided that the fiber is long enough for a complete pump-sideband collision, BS enables the generation of entanglement, or HOM interference, between photons with different carrier frequencies and wave packets, and photon FC, or entanglement swapping, with simultaneous wave-packet reshaping that is limited only by the available pump shapes (wave forms). Since arbitrary pump-wave-form generation is possible [22], the future of FC by BS looks bright.

[1] *Optical Code Division Multiple Access: Fundamentals and Applications*, edited by P. R. Prucnal (CRC Press, Boca Raton, FL, 2005).

[2] P. J. Winzer and R. J. Essiambre, Proc. IEEE **94**, 952 (2006).

[3] S. Tanzilli, W. Tittel, M. Halder, O. Alibart, P. Baldi, N. Gisin, and H. Zbinden, Nature (London) **437**, 116 (2005).

[4] H. J. Kimble, Nature (London) **453**, 1023 (2008).

[5] C. K. Hong, Z. Y. Ou, and L. Mandel, Phys. Rev. Lett. **59**, 2044 (1987).

[6] H. P. Specht, J. Bochmann, M. Mucke, B. Weber, E. Figueroa, D. L. Moehring, and G. Rempe, Nat. Photonics **3**, 469 (2009).

[7] M. G. Raymer, S. J. van Enk, C. J. McKinstrie, and H. J. McGuinness, Opt. Commun. **283**, 747 (2010).

[8] C. Belthangady, C.-S. Chuu, I. A. Yu, G. Y. Yin, J. M. Kahn, and S. E. Harris, Phys. Rev. Lett. **104**, 223601 (2010).

[9] J. Huang and P. Kumar, Phys. Rev. Lett. **68**, 2153 (1992).

[10] A. P. VanDevender and P. G. Kwiat, J. Mod. Opt. **51**, 1433 (2004); M. A. Albota and F. N. C. Wong, Opt. Lett. **29**, 1449 (2004); R. V. Roussev, C. Langrock, J. R. Kurz, and M. M. Fejer, *ibid.* **29**, 1518 (2004).

[11] D. Kielpinski, J. F. Corney, and H. M. Wiseman, Phys. Rev. Lett. **106**, 130501 (2011).

[12] B. Brecht, A. Eckstein, A. Christ, H. Suche, and C. Silberhorn, New J. Phys. **13**, 065029 (2011).

[13] C. J. McKinstrie, J. D. Harvey, S. Radic, and M. G. Raymer, Opt. Express **13**, 9131 (2005).

[14] H. J. McGuinness, M. G. Raymer, C. J. McKinstrie, and S. Radic, Phys. Rev. Lett. **105**, 093604 (2010).

[15] C. H. Kwok, B. P. P. Kuo, and K. K. Y. Wong, Opt. Express **16**, 10894 (2008).

[16] E. Myslivets, N. Alic, S. Moro, B. P. P. Kuo, R. M. Jopson, C. J. McKinstrie, M. Karlsson, and S. Radic, Opt. Express **17**, 11958 (2009).

[17] C. K. Law, I. A. Walmsley, and J. H. Eberly, Phys. Rev. Lett. **84**, 5304 (2000).

[18] R. A. Campos, B. E. A. Saleh, and M. C. Teich, Phys. Rev. A **40**, 1371 (1989).

[19] R. E. Giacone, C. J. McKinstrie, and R. Betti, Phys. Plasmas **2**, 4596 (1995). The characteristic transformations and derivations of the Green functions are described in the Appendix. If one changes unstable coupling to stable coupling, the modified Bessel functions become regular Bessel functions.

[20] The stable Green functions were stated explicitly in M. G. Raymer, J. Mod. Opt. **51**, 1739 (2004).

[21] H. J. McGuinness, M. G. Raymer, and C. J. McKinstrie, Opt. Express **19**, 17876 (2011).

[22] S. J. Cundiff and A. M. Weiner, Nat. Photonics **4**, 760 (2010).